J Mater Sci (2011) 46:5859–5875
DOI 10.1007/s10853-011-5543-3

Experimental studies on process-induced morphological characteristics of macro- and microstructures in laser consolidated alloys

Jianyin Chen · Lijue Xue · Sheng-Hui Wang

Received: 23 November 2010 / Accepted: 6 April 2011 / Published online: 27 April 2011

Abstract Laser consolidation (LC) developed by National Research Council's Industrial Materials Institute (NRC-IMI-London) since mid-1990s, is a laser cladding based rapid manufacturing and material additive process that could fabricate a "net-shape" functional metallic shape through a "layer-upon-layer" deposition directly from a computer aided design model without using molds or dies. In order to evaluate the LC processability of different materials, some representative nickel-based superalloys (IN-625, IN-718, IN-738, and Waspaloy), stainless steels (austenitic SS316L and martensitic SS420), and lightweight alloys (Ti–6Al–4V titanium alloy and Al-4047 aluminum alloy) have been investigated. Like other laser cladding based processes, due to process-induced rapid directional solidification, the LC alloys have demonstrated certain unique morphological characteristics. Moreover, the "as-consolidated" LC alloys, in nature, are in the "as-quenched" state, and some precipitation processes from their matrices, which are sometimes critical to the development of mechanical performance of the materials, could be effectively suppressed or retarded. Post-heat treatments, therefore, could necessarily facilitate the process of achieving their required operational microstructures. In this article, a comprehensive investigation was performed including metallurgical soundness and process-induced morphological characteristics of the LC materials, and microstructure development brought by post-LC heat treatments using optical microscope, scanning electron microscope, and X-ray diffraction. The implications on the mechanical performance of the LC materials were discussed as well in order to provide essential information for potential industrial applications of the LC materials.

J. Chen (✉) · L. Xue
Industrial Materials Institute, National Research Council of Canada, 800 Collip Circle, London, ON N6G 4X8, Canada
e-mail: jianyin.chen@nrc.gc.ca

S.-H. Wang
Chalk River Laboratories, Atomic Energy of Canada Limited, Chalk River, ON K0J 1J0, Canada

Introduction

Several rapid manufacturing processes using laser powder deposition have been independently developed by various organizations across the world, including laser engineered net shaping (LENS^{TM}) (Sandia National Laboratory) [1, 2], direct light fabrication (DLF) (Los Alamos National Laboratory) [3], direct laser deposition (DMD) (The University of Michigan) [4–6], laser direct casting (LDC) (The University of Liverpool) [7], and others since the mid-1990s of the last century. Nevertheless, the similarities of these processes are that all of them are laser cladding based material additive processes [8] whereas their differences lie in each individual process with its own unique system configuration (laser type, laser operating mode, laser processing head, and others) and process condition, which further differentiates the process capability and productivity, surface quality and dimensional accuracy for the shape (components, parts or tooling) thus fabricated, morphologies of macro- and microstructures, and mechanical performance of the processed materials. Consequently, each of the processes might address different industrial demands [9–16]. Furthermore, the majority of these processes might only produce "near-net" shape with rough surface finish and low dimensional accuracy, and additional machining could be a must to achieve the desired surface finish and dimensional accuracy for the final products [17], which, more or less, could reduce the attractiveness of these processes.

In contrast, laser consolidation (LC) process, being developed by NRC-IMI-London since mid-1990s, utilizes unique process condition and system configuration (such as pulsed laser, proprietary processing head, and others) that enable fabrication of "net-shape" functional product with excellent surface finish and dimensional accuracy in one step [18]. This material additive process, in essence, can directly fabricate metallic shape through computer aided design (CAD) model. The shape thus obtained does not require further surface machining [19], which, therefore, offers unique opportunities to reduce manufacturing time in many potential applications such as complex three dimensional shapes that are difficult to fabricate by conventional manufacturing processes. For instance, Xue et al. [20] demonstrated that some complex flextensional transducer shells have been successfully fabricated using LC process after numerous failures with other existing manufacturing technologies. Moreover, this LC process offers other advantages including reduced cost, minimal wastage of materials, and flexibility for design changes, etc. The LC process can also be used to repair/refurbish damaged high-value components, parts, or tooling to restore their original geometries and functionalities, and extend their service life with affordable cost. The LC components, parts, or tooling can minimize or even eliminate the usages of conventional welding processes that potentially induce hot cracks in the weld metal and liquidation cracks in the heat-affected zone for certain alloys. Recently, the LC process has been used to build functional parts (or structures) for mold and die applications such as plastic injection nozzles with embedded multiple cooling channels [21]. Xue [19] has made an excellent technical overview on applying LC process to directly manufacture various industrial components, parts, and tooling. Figure 1 presents some of demonstrated LC pieces produced in NRC-IMI-London.

Within a span of more than past 10 years, much study has been done on metallurgical soundness and morphological characteristics of numerous LC alloys including nickel-based high-temperature alloys (IN-625, IN-718, IN-738, and Waspaloy), stainless steels (austenitic SS316L and martensitic SS420), and lightweight alloys (Ti–6Al–4V titanium alloy and Al-4047 aluminum alloy) which have shown a range of potential applications in aerospace, defense, automotive, medical devices, and other manufacturing industries. Some of these materials have also been investigated by other laser-aided materials additive processes (such as LENS and DMD, etc.) as well [1–7, 22–27]. However, since most of these processes only produce shapes in "near-net", their process conditions and system configurations could be quite different from the LC process. These differences could bring certain different macro- and microstructures to LC alloys, which might affect the resulting mechanical performance of the materials. For example, due to process-induced rapid directional solidification, some nickel-based LC alloys exhibit coarse columnar grains in combination with refined directionally solidified dendrites inside; moreover, the LC alloys in "as-consolidated" condition are naturally in "as-quenched" state, with a consequence that, in some cases, the LC alloys cannot directly be utilized without further post-heat treatments to achieve their required operational microstructures [28].

Fig. 1 Examples of shapes (components, parts, and tooling) fabricated by LC technology (www.nrc-cnrc.gc.ca/imi-imi)

Therefore, this study is an attempt to have a comprehensive understanding and to explore potential possibilities of controlling the macro- and microstructures of the LC materials in order to achieve their required mechanical performance at desired service conditions, and to provide more process confidences and potential industrial applications in terms of LC-produced shapes (such as components, parts, or tooling). Furthermore, the similarities and differences in the LC macro- and microstructures among different material groups and their evolution brought by post-heat treatments have been studied, and potential impacts on the mechanical performance of those LC materials were discussed as well.

Experimental

Materials

The Table 1 summarized the selected materials and their characteristics used for the current LC study. The commercial spherically shaped gas-atomized IN-625 (commercial name: NI-328), IN-718 (NI-202), IN-738 (NI-284), and Waspaloy (NI-492) alloy powders (Praxair Surface Technologies, Indianapolis, IN), SS316L (Diamalloy 1003) alloy powder (Sulzer Metco Inc., Westbury, NY), SS420 (FE-211-1) alloy powder (Praxair Surface Technologies, Indianapolis, IN), Ti–6Al–4V alloy powder (Advanced Powders and Coatings Inc., Boisbriand, PQ, Canada), and Al-4047 (Al–Si) alloy powder (Valimet, Inc., Stockton, CA) were used as LC materials. The size of these powders ranged between 10 and 55 μm in diameter and their chemical compositions were summarized in Table 2. Since the carbon content in Praxair's FE-211-1 powder (nominally referred as to AISI SS410 steel by the manufacturer) was high (~0.5 wt%) and actually within the nominal carbon content of AISI SS420 steel, the authors regarded this powder as AISI SS420 steel in the article instead.

Laser consolidation process

Laser consolidation process with blown powder feeding was used for the present study. In the process setup illustrated in Fig. 2a, a 0.5–1 kW pulsed Nd:YAG laser in combination with a precision powder feeder and a computer numerically controlled (CNC) motion system was utilized. The laser focusing optics and the powder feeding nozzle were installed on the *Z*-axis of the CNC motion system while one substrate (the length and width of the substrate would depend on the shape to be built; the thickness of the substrate was about 10–15 mm) was mounted on the X–Y motion table. The LC process was carried out in a glove box filled with argon to maintain a low oxygen level (less than 50 ppm) and in addition, the argon was also used as carrying gas for the delivery of alloy powder and shielding gas for the protection of the laser optics. During the LC process, the pulsed laser beam (with an average power of several tens to several hundreds watts) was focused onto the substrate to create a melt pool (between 0.5 and 1.0 mm in diameter) while the alloy powder was simultaneously injected into the pool. As the laser beam (or substrate) moved at a traverse speed of about 2–10 mm/s following a CAD model through a predesigned "laser tool" path, the molten material was rapidly re-solidified to form the first layer of the shape, which was metallurgically bonded to the substrate. The successive layer was, then, deposited on the top of the preceding layer through re-melting of a thin portion of that layer and re-solidified together with the injected powder. This "layer-upon-layer" deposition was repeated until the desired shape was formed (such as the one shown in Fig. 2b).

Post-heat treatments

During the LC process, the size of the melt pool (normally between 0.5 and 1.0 mm in diameter) was significantly smaller than the dimensions of the underneath substrate and the wall being built that consequently acted as a huge "heat sink" to the melt, leading to a rapid quenching of the LC material immediately after solidification. Hence, for some LC materials, proper post-heat treatments might be essential to achieve their required operational microstructures. Table 3 summarized the post-heat treatments used in this investigation.

Characterization

After the process, the LC specimens were mechanically cross-sectioned and polished down to less than 1 μm for

Table 1 Selective alloys and their characteristics for the current LC study [29–32]

Material	Characteristics
IN-625	Ni-based solid solution strengthened superalloy that has excellent corrosion resistance, oxidation resistance, outstanding strength, and toughness in the temperature range up to 1093 °C
IN-718	Ni-based age-hardenable superalloy with corrosion resistance, high strength, excellent high-temperature creep rupture strength, and outstanding weldability
IN-738	Ni-based age-hardenable superalloy with excellent creep strength and hot corrosion resistance
Waspaloy	Ni-based age-hardenable superalloy with high-temperature strength and good corrosion resistance
SS316L	Low carbon molybdenum-bearing austenitic stainless steel with no carbide precipitation at grain boundaries and has a better weldability; the alloy has better toughness, high creep, stress to rupture, and tensile strength at elevated temperature as well
SS420	Martensitic stainless steel with high strength and corrosion resistance
Ti-6Al-4V	A α-β type Ti-based alloy with an excellent combination of strength and toughness along with excellent corrosion resistance
Al-4047	Aluminum–silicon (Al–Si) alloy with excellent weldability

Table 2 Chemical compositions of the alloy powders provided by the manufacturers

Alloy	IN-625	IN-718	IN-738	Waspaloy	SS316L	SS420	Ti–6Al–4V	Al-4047
Chromium	22.0	19.0	16.1	19.1	16.4	14.0	0.02	–
Molybdenum	9.0	3.0	1.77	4.2	2.23	–	–	–
Tungsten	–	–	2.59	–	–	–	–	–
Tantalum	3.7	–	1.74	–	–	–	–	–
+Niobium		5.0	0.86	–	–	–	–	–
Zirconium	–	–	0.06	–	–	–	–	–
Manganese	–	–	–	–	1.42	0.37	–	–
Vanadium	–	–	–	–	–	–	3.94	–
Copper	–	–	–	–	–	–	–	0.01
Silicon	–	–	–	–	0.45	1.0	–	11.41
Magnesium	–	–	–	–	–	–	–	0.02
Boron	–		0.011	–	–	–	–	–
Carbon	0.03	0.05	0.10	–	0.024	0.5	0.07	–
Nitrogen	–	–	–	–	–	–	0.01	–
Oxygen	–	–	–	–	–	–	0.13	–
Aluminum	–	–	3.27	1.1	–	–	6.18	Bal.
Cobalt	–	–	8.34	13.1	–	–	–	–
Titanium	–	–	3.38	2.9	–	–	Bal.	–
Iron	0.4	17.0	–	0.049	Bal.	Bal.	0.10	0.17
Nickel	Bal.	Bal.	Bal.	Bal.	10.4	–	0.02	–

metallographic examination. The macro- and microstructures of the LC alloys were revealed using proper chemical etchants. An Olympus optical microscope (OM) was used to study overall macro- and microstructures of the LC specimens. A Hitachi variable pressure scanning electron microscope along with an Oxford energy dispersive spectrometer (VP-SEM/EDS) was used to investigate the microstructures under high resolution. A Philips X'Pert X-ray diffractometer (XRD) was employed to identify phases presented in the LC specimens. The microhardness of the LC specimens was measured on a Buehler microhardness tester using a Vickers indentor. And a 100 kN Instron mechanical testing system was used to evaluate tensile properties of the LC materials as per ASTM E8-04.

Results and discussion

Macro- and microstructures in "as-consolidated" LC alloys

Morphological characteristics of solidified structures

It was found that all the thin-walled LC specimens sectioned along their wall build-up directions exhibited layer-wise morphologies with no exception (Figs. 3, 4, 5, 6), which truly reflected the nature of the "layer-upon-layer" based LC process. Nevertheless, there were still some different details in their solidified structures among the different LC material groups, which, in certain way, also reflected different solidification behaviors of the materials under LC process-induced thermal conditions.

For the nickel-based LC alloys (IN-625, IN-718, IN-738, and Waspaloy), both grains and dendrites, which spanned multiple deposited layers, grew almost parallel to their wall build-up directions. For instance, Fig. 3a, c, and e presents the solidified structures of the "as-consolidated" LC IN-718, LC IN-738, and LC Waspaloy sectioned along their wall build-up directions: non-uniform coarse columnar grains with dominant fine directionally solidified dendrites (including a few cellular colonies) inside. These solidified structures reflected a kind of epitaxial growth of dendrites during a rapid directional solidification. The XRD results of the "as-consolidated" LC IN-625, LC IN-718 (Fig. 3b), LC IN-738 (Fig. 3d), and LC Waspaloy (Fig. 3f) revealed the presence of a directionally solidified structure aligned with $\langle 100 \rangle$ crystallographic direction in their f.c.c.-structured γ matrices, which was almost parallel to the wall build-up direction as well. Table 4 summarized the ratios of the XRD integral intensities of selective diffraction lines ($I_{\gamma(200)}/I_{\gamma(111)}$ for the LC superalloys) to characterize the degree of preferred orientation presented in the LC materials, in which the XRD pattern of the respective powder was treated as a baseline for the respective homogenous and randomly orientated polycrystalline material. Both the optical morphologies and

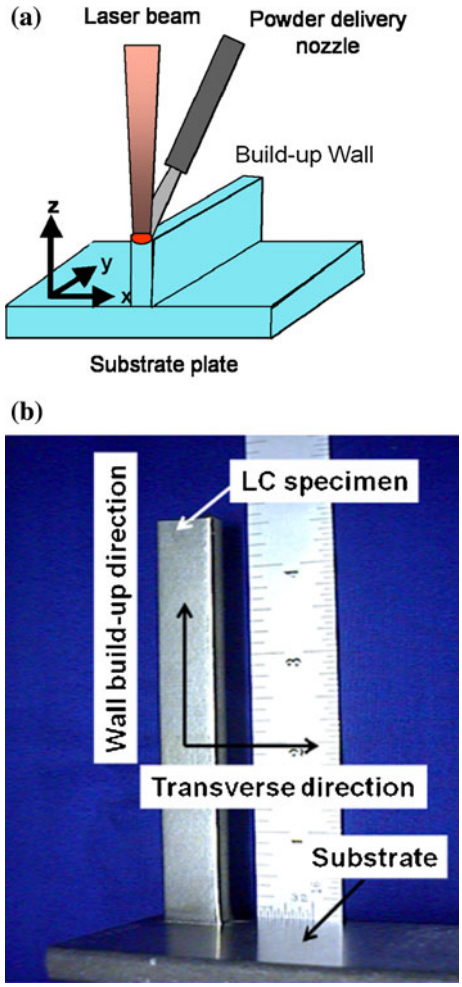

Fig. 2 **a** An illustration of the LC process and **b** a LC thin-walled structure (IN-738) for the current material characterization

XRD measurements of the nickel-based LC alloys were fully in agreement with the presence of preferred orientation.

For the LC stainless steels including austenitic SS316L and martensitic SS420, their chemical compositions and thermal conditions have led to different avenues of liquid–solid phase transformation during solidification, resulting in different solidified structures. The "as-consolidated" LC SS316L sectioned along the wall build-up direction exhibited coarse columnar grains with dominant refined cellular structure (plus a few fine directional dendrite colonies) inside, which spanned several deposited layers (Fig. 4a). The XRD pattern (Fig. 4b) indicated that the major phase presented in the "as-consolidated" LC SS316L was a slightly preferred orientated austenitic phase (γ) since the XRD pattern of the LC alloy has shown a slightly higher ratio of the integral intensities of the diffraction lines of $I_{\gamma(200)}/I_{\gamma(111)}$ with about 0.7 as compared to the respective powder (about 0.5) (see Table 4). Comparatively, the "as-consolidated" LC SS420 sectioned along the wall build-up direction, on the other hand, showed that each deposited layer actually contained two sub-layers: one with dominated directionally solidified dendritic structure (a major portion of the layer) along the wall build-up direction and another with fine equiaxial cellular structure (a small portion of the layer) (Fig. 4c). Moreover, the continuity of the solidified structure has been broken between two adjacent layers. Unlike the nickel-based LC alloys and LC SS316L, it was hard to recognize any grain boundaries in the "as-consolidated" LC SS420. The XRD analysis (Fig. 4d) revealed that the phases presented in the "as-consolidated" LC SS420 were martensitic α phase along with a substantially high amount of retained austenitic γ' phase (about 53.9 vol.%). Nevertheless, there was still a slightly preferred orientation in the α phase as well as the γ' phase since the LC SS420 exhibited slightly higher ratios of the integral intensities of the diffraction lines of $I_{\alpha(110)}/I_{\alpha(200)}$ and $I_{\gamma'(200)}/I_{\gamma'(111)}$ with about 15.7 and 0.6, respectively, as compared to the corresponding powder (about 13.6 and 0.4, respectively) (Table 4).

The morphology of solidified structure in the LC Al-4047 aluminum alloy sectioned along the wall build-up direction (Fig. 5a) was similar to the "as-consolidated" LC SS420 (Fig. 4c). The XRD pattern of the LC Al-4047 (Fig. 5b) revealed the presence of a majority of f.c.c.-structured α-Al phase and a small amount of Si phase. The α-Al phase showed a high degree of preferred orientation

Table 3 Post-heat treatments (HTs) for the LC materials where the SHTs represent the recommended standard heat treatments employed in industry [33]

LC Material	Heat treatment (HT) schedule
IN-625	600 °C/72 h, 700 °C/72 h, 800 °C/72 h, 900 °C/72 h, and 1100 °C/2 h with air cooling, respectively
IN-718	980 °C/1 h + 720 °C/8 h + 620 °C/8 h with air cooling (SHT)
IN-738	1120 °C/2 h + 845 °C/24 h with air cooling (SHT)
Waspaloy	1079 °C/4 h + 843 °C/4 h + 760 °C/16 h with air cooling (SHT)
SS316L	Annealed at (a) 538 °C/24 h and (b) 871 °C/24 h with air cooling
SS420	(a) Tempered at 316 °C/2 h and (b) re-austenitized at 1008 °C/0.5 h and quenched in oil, and then tempered at 316, 427, 457, 477, 497, 538, and 600 °C for 2 h, respectively

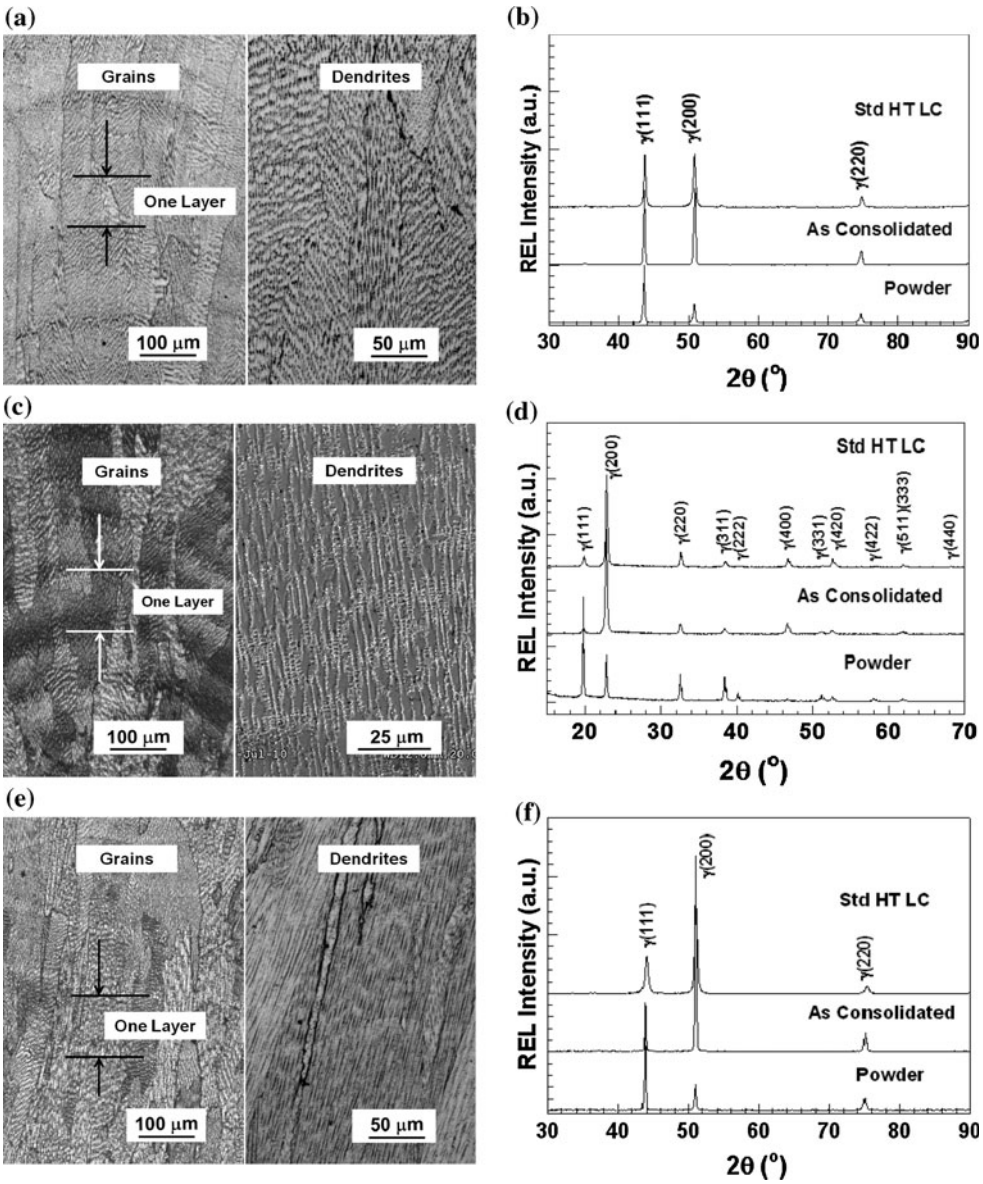

Fig. 3 **a**, **c**, and **e** Layer-wise morphologies of solidified structures in "as-consolidated" LC IN-718, LC IN-738, and LC Waspaloy; **b**, **d**, and **f** XRD patterns of powdered, "as-consolidated" LC, and standard heat-treated (SHT) LC IN-718 (CuK_α), LC IN-738 (MoK_α), and LC Waspaloy (CuK_α). All the LC specimens were sectioned along the wall build-up directions, showing non-uniform coarse columnar grains with dominant fine directionally solidified dendrites inside; whereas their major phase was f.c.c.-structured γ phase with preferred $\langle 100 \rangle$ orientation

because the ratio of the integral intensities of the selective diffracted lines of $I_{\alpha(200)}/I_{\alpha(111)}$ was about 3.7, which was much higher than the respective powder (about 0.5) (Table 4).

The "as-consolidated" LC Ti–6Al–4V titanium alloy showed quite different solidified structure: although the morphology of the LC alloy sectioned along the wall build-up direction still revealed a layer-wise structure in combined with spanning-multiple-layer coarse columnar grains (Fig. 6a) with acicular phase inside (Fig. 6b), there was no presence of fine directionally solidified dendrites. Figure 6c exhibits the same coarse columnar grains obtained by sectioning transversely to the wall build-up direction, which appeared as equiaxial grains, but actually were the cross-sectioned view of the columnar grains. The XRD pattern of the LC Ti–6Al–4V (Fig. 6d) indicated the main phase presented in the "as-consolidated" LC Ti–6Al–4V was h.c.p.-structured martensitic α' phase. As compared to the wrought material, Ti–6Al–4V in both gas-atomized powder and "as-consolidated" form showed a single martensitic α' phase without any β phase, presumably due to the rapid solidification and quenching induced by both processes. Moreover, as expected, there was a preferred orientation in the martensitic α' matrix in the LC Ti–6Al–4V, which was inherent from the prior-β columnar grains, since the LC alloy exhibited a higher ratio of the integral intensities of the selective diffraction lines of $I_{\alpha'(002)}/I_{\alpha'(100)}$ with about 2.6 as compared to the respective powder (about 0.9) (Table 4).

Table 5 summarized the primary/secondary dendritic arm spacing (PDAS/SDAS) and cell spacing (CS) of some LC materials, which indicated that the LC materials

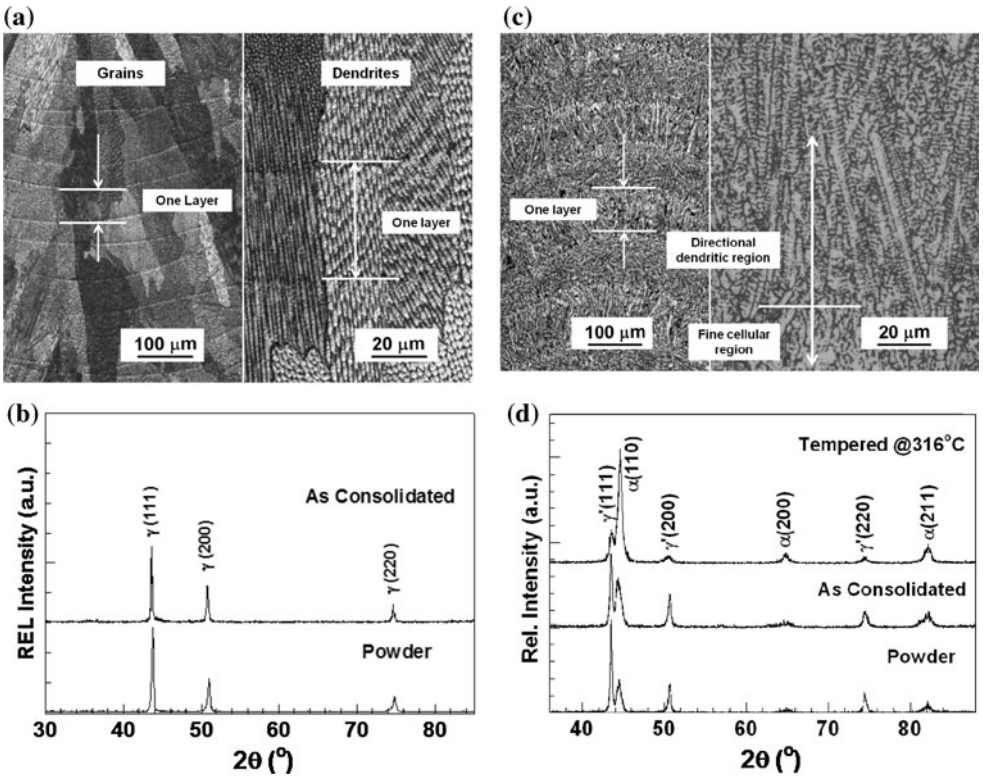

Fig. 4 Layer-wise morphologies of solidified structures in "as-consolidated". **a** austenitic LC SS316L: coarse columnar grains with dominant fine equiaxial cellular structure (a few directional dendrite colonies) inside, and **c** martensitic LC SS420: two sub-layers within one deposited layer—one with predominated directionally solidified dendrites and another with fine equiaxial cellular structure. Both LC specimens were sectioned along the wall build-up directions. The XRD patterns of **b** powdered and "as-consolidated" LC SS316L (CuK_α), and **d** powdered, "as-consolidated", and "tempered at 316 °C" LC SS420 (CuK_α)

experienced a rapid solidification, leading the refined solidified structures to most of them.

Phases and microstructures

With combined analyses of OM, SEM/EDS, and XRD, the major phases presented in the "as-consolidated" LC materials can be identified.

For the nickel-based LC alloys including IN-625, IN-718, IN-738, and Waspaloy, the major phase in "as-consolidated" condition was γ matrix. It was also revealed that some primary carbide precipitated along the interdendritic and intradendritic regions (such as the cases shown in Fig. 7a, b). On the other hand, the rapid self-quenching after solidification could result in a supersaturated γ solid solution, which has been proven for the LC IN-718, LC IN-738, and LC Waspaloy, since the high-resolution SEM images of those "as-consolidated" LC alloys showed little evidence of the presence of any γ' (or γ'') particles in their γ matrices. Post-heat treatments, hence, were required to ensure these age-hardenable LC alloys to achieve their full precipitations.

For the austenitic LC SS316L, Fig. 7c shows that the "as-consolidated" steel has a mixed fine γ cells/dendrites with a dominance of cellular structure. For the martensitic LC SS420, Fig. 7d shows that the "as-consolidated" steel has a dendritic morphology with no obvious martensitic characteristics, and carbide particles existed at both interdendritic and intradendritic regions. As mentioned, a considerable amount of retained austenite (γ') remained in the "as-consolidated" LC SS420 (about 53.9 vol.%). This might be attributed to rapid solidification and dissolution of a large amount of carbides into the steel during the molten stage, which caused the depression of martensitic start temperature (M_s), leading to a less amount of martensite (α) in resulting duplex phases ($\alpha + \gamma'$) than that would be predicted for conventionally treated material. The process-induced high amount of retained austenite in the LC SS420 is usually unstable and may be transformed during service, causing dimensional change, brittleness, or even cracking. Consequently, it is desirable to eliminate it through post-heat treatments before usage.

For the "as-consolidated" LC Al-4047 alloy, as shown in Fig. 7e, fine dendritic structure existed with the primary α-Al phase as well as laminar-type eutectic (α-Al + Si) structure at the interdendrites.

The "as-consolidated" LC Ti–6Al–4V microstructure showed acicular martensitic α' phase (Fig. 7f), and no other phase can be observed along grain boundaries. In general, the microstructure of Ti–6Al–4V alloy depends upon the cooling conditions employed upon the high-temperature β form of the alloy. A typical "as-cast" Ti–6Al–4V microstructure consists of transformed β containing acicular α as well as α at prior-β grain boundaries, while an annealed wrought Ti–6Al–4V bar typically consists of equiaxed α grain plus intergranular β [31]. The lack of β phase in the

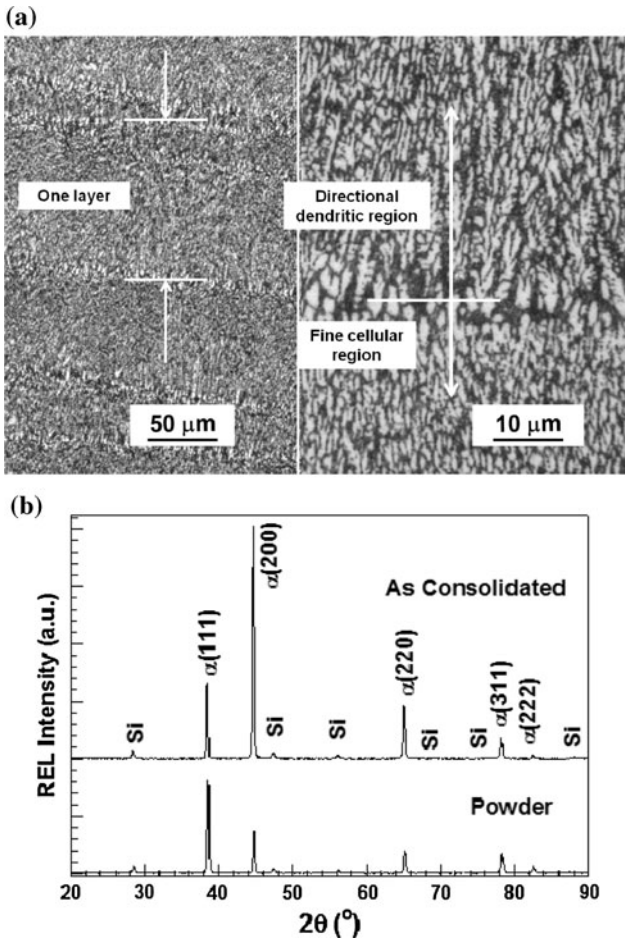

Fig. 5 **a** A layer-wise morphology of solidified structure in "as-consolidated" LC Al-4047 alloy sectioned along the wall build-up direction. Two sub-layers within each deposited layer: one with predominated directionally solidified dendritic structure and another with fine equiaxial cellular structure. **b** XRD patterns of powdered and "as-consolidated" LC Al-4047 alloy (CuK_{α})

"as-consolidated" LC Ti–6Al–4V is attributed to the high cooling rate (rapid quenching) inherent to the LC process.

LC solidification process

It is well known that laser cladding based processes (including the LC process) induce rapid directional solidification as suggested by the morphological characteristics of the solidified structures in the materials thus produced. More specifically regarding the LC process, a melt created by a pulsed laser beam (with a pulse duration of several milliseconds) only has a diameter of 0.5–1.0 mm, dimension-wise much larger substrate and the LC wall being built would act effectively as a huge "heat sink" to rapidly extract the latent heat generated during the solidification of the melt and dissipate through the solidified phase(s) parallel but opposite to the wall build-up direction (which was the maximum temperature gradient as well). This would lead to a rapid directional solidification and subsequent rapid quenching for the melt. In addition, as compared to other laser cladding based rapid manufacturing processes such as LENS and DMD in which continuous wave lasers are frequently used as their heat sources [1–7], the pulsed laser used in the LC process is associated with relatively high peak power but with low heat input [18, 19], which induces different thermal patterns on the solidification of LC materials [34]. That is, the melt of a LC material could be created within an extremely short period of pulse duration (several milliseconds), and there is no heat input between two consecutive pulses, which could result in a much faster cooling rate for the melt. Pryds [35] pointed out that the measured PDAS/SDAS or CS of microstructure could be used to estimate cooling rate of a material during solidification. Marsden et al. [36] had measured dendritic CS produced by laser melting of SS420 steel and concluded that with an order of 3–4 μm the melt was solidified at a cooling rate of more than 10^3 °C/s from the liquid phase. For the present LC SS420 steel, the CS was about 3.7 μm, which, therefore, appeared to have a comparable cooling rate of 10^3 °C/s as well.

Like any "as-cast" materials, the morphologies of the LC-solidified structures embedded thermal histories of the solidification process. For instance, the nickel-based LC alloys (IN-625, IN-718, IN-738, and Waspaloy) occurred with the dominated spanning-multiple-layer epitaxial dendrites; the austenitic LC SS316L was dominated with extremely fine cellular structure; the martensitic LC SS420 and LC Al-4047 aluminum alloy showed that, within each deposited layer, there were a thin layer of fine equiaxial cells plus a large amount of directionally solidified dendrites; and the LC Ti–6Al–4V titanium alloy showed coarse directional columnar structure with no presence of cells/dendrites inside. These morphological characteristics, more or less, reflected their actual thermal conditions during solidification. In this study, the authors attempted to use phenomenological approach to explain what might have happened in the LC solidification process although a full understanding of the solidification behaviors in these LC materials induced by the pulsed laser might need an in-depth experimental study combined with solidification modeling/simulation.

In most cases, for the deposition of the first layer, the LC materials would go through a process of nucleation and directional growth of crystallites. When a pulsed laser beam melted a portion of substrate in combination with injected powder (i.e., LC material) to form a melt (0.5–1.0 mm in diameter), a substantially high thermal undercooled layer would be created in the melt ahead of solid/liquid interface due to the substrate-induced "heat sink" effect, which would promote to form a small layer of fine nuclei at the interface. With the nucleation and growth,

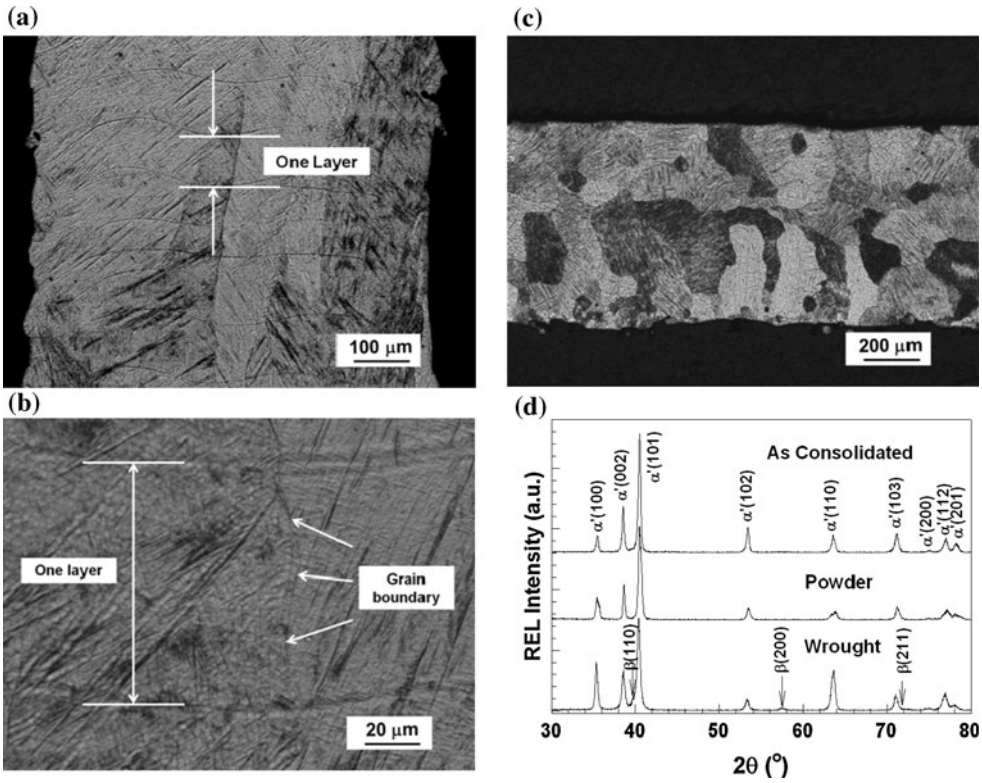

Fig. 6 **a**, **b** A layer-wise morphology of solidified structure in "as-consolidated" LC Ti–6Al–4V alloy sectioned along the wall build-up direction: spanning-multiple-layer coarse columnar grains with acicular α' phase inside; **c** the morphology of "as-consolidated" LC alloy sectioned transversely to the wall build-up direction, and **d** XRD patterns of wrought, powdered, and "as-consolidated" LC Ti–6Al–4V alloy (CuK_α)

Table 4 Summary of XRD integral intensities of selective diffraction lines to characterize the degree of preferred orientations in LC materials sectioned along the wall build-up direction

LC material	Condition	$I_{\gamma(200)}/I_{\gamma(111)}$ (γ phase)	$I_{\gamma'(200)}/I_{\gamma'(111)}$ (γ' phase)	$I_{\alpha(110)}/I_{\alpha(200)}$ (α phase)	$I_{\alpha(200)}/I_{\alpha(111)}$ (α phase)	$I_{\alpha'(002)}/I_{\alpha'(100)}$ (α' phase)
IN-625	Powder	0.5				
	As consolidated	3.7				
	900 °C/72 h	1.7				
IN-718	Powder	0.5				
	As consolidated	1.2				
	SHT	1.0				
IN-738	Powder	0.5				
	As consolidated	15.8				
	SHT	15.8				
Waspaloy	Powder	0.5				
	As consolidated	15.3				
	SHT	2.1				
SS316L	Powder	0.5				
	As consolidated	0.7				
SS420	Powder		0.4	13.6		
	As consolidated		0.6	15.7		
Ti–6Al–4V	Powder					0.9
	As consolidated					2.6
Al-4047	Powder				0.5	
	As consolidated				3.7	

Table 5 Average primary/secondary dendritic arm spacing (PDAS/SDAS) and cell spacing (CS) of "as-consolidated" LC alloys

LC alloy	PDAS (μm)	SDAS (μm)	CS (μm)
IN-625	~2.1	~1.2	–
IN-718	~3.7	–	~3.8
IN-738	~3.1	~1.7	–
Waspaloy	~2.7	–	~2.3
SS316L	~2.5	–	~2.5
SS420	~3.6	~1.6	~3.7
Al-4047	~1.1	~ 0.9	~1.1

the latent heat of solidification (or the heat of fusion) would be generated at the interface and dissipated rapidly and directionally through the solidified phase (opposite to the wall build-up direction) to create a rapid directional solidification condition for the growth of the nuclei. Simultaneously supersaturated solute atoms would be rejected from the phase just being solidified into the melt ahead of the solid/liquid interface, if the solute partition coefficient (k_0) was less than unity (most of the LC materials satisfied this condition except LC Ti–6Al–4V alloy [25]) and created a constitutionally undercooled melt layer ahead of the advancing solid/liquid interface, which could pose a perturbation at the prior stable planar interface and potentially lead to formation of cellular or columnar dendrites in the melt depending on the solidification rate [37].

Mostly, the nuclei just formed ahead of the interface would rapidly grow into columnar dendrites (such as LC IN-625, LC IN-718, LC IN-738, and LC Waspaloy) almost parallel but opposite to direction of the heat flow (maximum temperature gradient) which was the direction of preferred crystallographic growth of the dendrites ($\langle 100 \rangle$ for f.c.c.-structured crystal) as well. However, when the solidification rate is very high, a transition from the growth of columnar dendrites to fine cellular structure could occur in the melt [37]. The morphology of solidified structure in the LC SS316L has shown such a pattern. This also resonated with the study of Lee et al. [38] in the microstructure map of directionally solidified Fe–18Cr stainless steels as function of solidification rate that the appearance of cellular structure could be either with relatively low or with extremely high solidification rate (such as laser deposition) while the presence of dendritic structures could be with the solidification rate in-between. Antonsson and Fredriksson [39] had a similar observation on the solidification of IN-718 alloy as well. In the present case, the pulsed laser (with a pulse duration of several milliseconds) might have introduced a much higher cooling rate (or high solidification rate) in the SS316L melt, which has pushed the solidification mode toward the region from fine dendritic to fine cellular structure.

In the subsequent layer deposition, there could be some different growth modes related to the epitaxial growth based on existing dendrites or re-nucleation and growth, depending on the nature of LC materials (for instance, the chemical and crystallographic compatibility between the new and the existing deposited layer) in addition to their thermal conditions. For the nickel-based LC alloys (IN-625, IN-718, IN-738, and Waspaloy), the primary solidification γ phase in the first layer once solidified would be rapidly quenched and remained as the same crystal structure at room temperature. When the second or subsequent layers were deposited onto the top of the first (or preceding) layer, a thin top portion of the first (or preceding) layer would be re-melted in combined with the injected powder to form a melt. The columnar dendrites in the new layer could have grown epitaxially from the columnar dendrites in the first (or preceding) layer, since the primary solidification phase (that was the γ phase) of the new layer being deposited has an identical crystal structure (probably chemical composition as well) with the first (or preceding) layer and thus, seemingly, the required free energy for the continued growth instead of new nucleation was minimal and the continued epitaxial growth could prevail. This was exactly what happened in the LC of the nickel-based alloys. In the end, the newly deposited layer would maintain the continuation and orientation of the prior columnar dendrites, which were almost aligned with the direction of the wall build-up direction, to form the directionally solidified structure that could span several deposited layers. The characteristics of the preferred orientation in the LC nickel-based alloys might be favored in certain aero-engine applications, such as for the repair and restoration of directionally solidified turbine blades.

Stainless steels (austenitic SS316L and martensitic SS420), however, could face multiple choices of primary solidification mode (either stable δ ferrite or metastable γ austenite), depending on chemical compositions of the alloys and their solidification conditions, which makes the solidification process of steels more complicated. Vilar et al. [40] and Colaco and Vilar [41, 42] found that primary γ solidification mode was kinetically favored for higher solidification rate (such as laser deposition) whereas primary δ solidification mode predominated at very low solidification rate (such as equilibrium solidification). Lin and Yue [43], Vilar et al. [40], and Colaco and Vilar [41, 42] had studied the solidification modes of SS316L in the laser rapid forming and DIN X42Cr13 (0.47 wt%C, 12.8 wt%Cr, Fe bal.) martensitic stainless steel (similar to SS420) in laser melting, respectively, and concluded that the growth of single metastable γ phase was the most favorable in both cases. It could be said that, hence, the primary solidification mode for both SS316L and SS420 in the LC process was the metastable γ phase. After

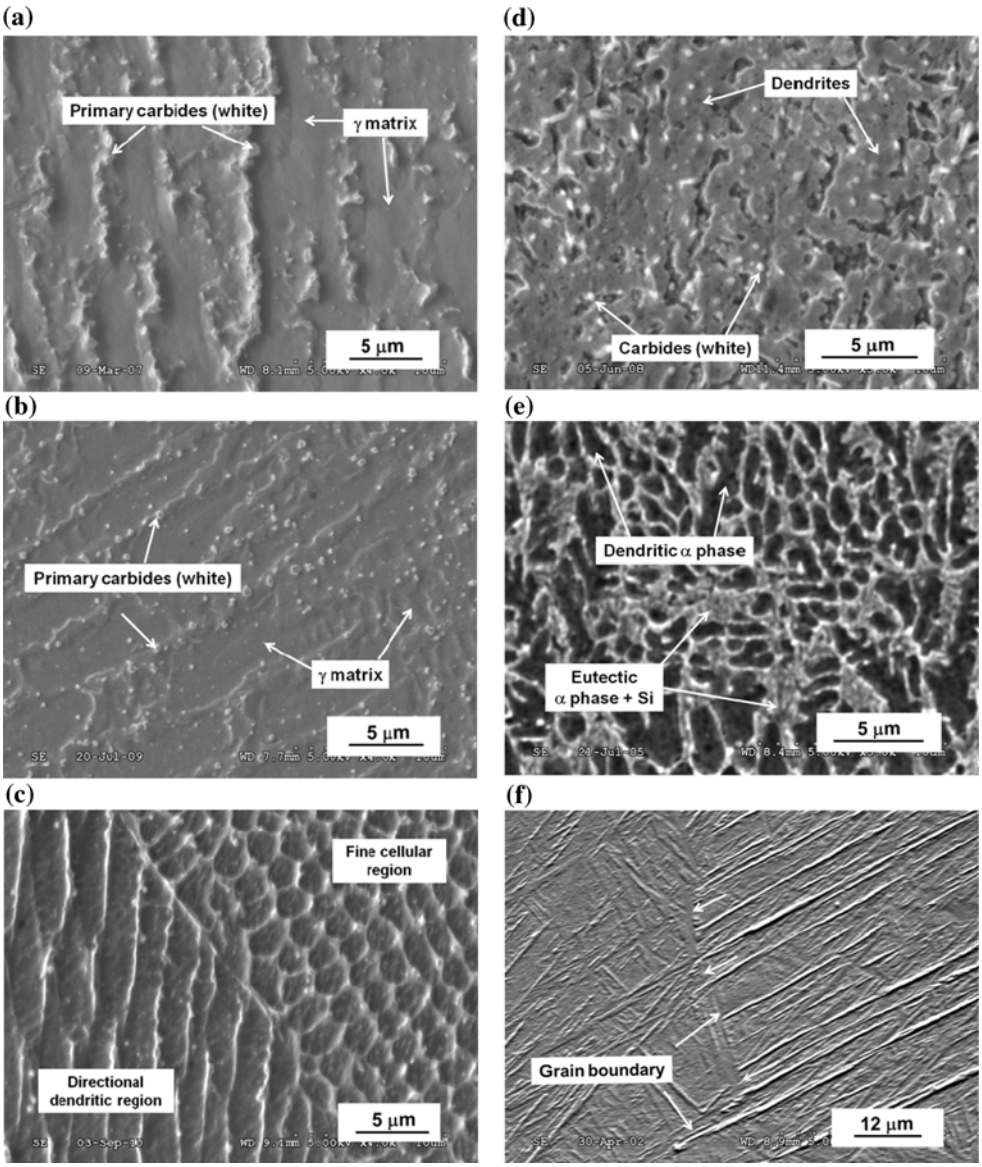

Fig. 7 SEM microstructures of **a** LC IN-718, **b** LC IN-738, **c** LC SS316L, **d** LC SS420, **e** LC Al-4047, and **f** LC Ti–6Al–4V alloys sectioned along the wall build-up directions

solidification, the LC SS316L would retain the high-temperature γ phase at room temperature; whereas the LC SS420 would experience a martensitic phase transformation ($\gamma \rightarrow \alpha + \gamma'$), in which the γ' phase was retained austenite. And the resulting LC SS420 presented duplex phases ($\alpha + \gamma'$) at room temperature.

Since the primary solidification phase (γ phase) of the LC SS316L would remain at room temperature, which should have a thermodynamic advantage to the epitaxial growth for the subsequent deposition of the new layers. However, the LC SS316L along the wall build-up direction has, in fact, shown the spanning-multiple-layer coarse columnar grains with dominated extremely fine cellular structure inside, probably because of the extremely rapid solidification rate, which favored to form a large amount of new nuclei. Only limited epitaxially grown colonies of directional solidified dendrites spanning several deposited layers could be observed in the LC SS316L, which contributed a weak preferred orientation parallel to the wall build-up direction in resulting microstructure.

In contrast, when depositing a new layer of the SS420, the primary solidification phase (γ phase) was not fully crystallographically compatible with the first (or preceding) layer (duplex phases $\alpha + \gamma'$ instead). Thus, the continued epitaxial growth of the columnar dendrites from the first (or preceding) layer seemingly has been disrupted, and re-nucleation ahead of the solid/liquid interface in the melt prevailed and some of them subsequently rapidly grew into

the melt to form directional columnar dendrites along the wall build-up direction but completely constrained within the layer. The resulting solidified morphology of the LC SS420 showed a large amount of directionally solidified dendrites adjacent to a thin layer of fine cells within each layer.

For the solidification process of LC Al-4047 aluminum alloy, f.c.c.-structured α-Al phase would be the primary solidification phase which remained at room temperature. During the continued cooling down, the residual liquid between the primary α-Al dendrites would be solidified to form eutectic phase (α-Al + Si). For the deposition of subsequent layer, seemingly, the formation of new nuclei at the highly undercooled melt ahead of the solid/liquid interface could be more favored than continually epitaxial growth of the dendrites from the first (or preceding) layer, possibly due to the chemical and crystallographic incompatibility between the new and the first (or preceding) layer (with primary α-Al phase plus eutectic phase α-Al + Si). Thus, a thin layer of cells was formed ahead of the interface in the melt, and similar to the LC SS420, some of the newly formed nuclei could rapidly grow preferably along the wall build-up direction to form the directionally solidified dendrites but constrained within the layer.

The solidification process of LC Ti–6Al–4V titanium alloy was slightly different, and the morphology of the solidified structure along the wall build-up direction showed spanning-multiple-layer coarse columnar prior-β grains with acicular martensitic α' phase inside. There was no presence of fine dendritic structure like other LC materials. Semiatin and Kobryn [44] had suggested that the thermal gradient parallel to the wall build-up direction during solidification of the laser additive manufactured Ti–6Al–4V material was very high relative to the solidification rate, and consequently the formation of new nuclei ahead of the advancing solid/liquid interface could be much less possible. In addition, Wu et al. [25] and Bontha et al. [45] found experimentally and theoretically that laser deposited Ti–6Al–4V preferred to grow into columnar grains under virtually all laser process conditions (different cooling rates) rather than re-nucleation, and suggested that since the primary solidified phase (b.c.c.-structured β phase) in the Ti–6Al–4V showed Ti-depletion, and the corresponding liquid phase showed Ti-enrichment as per its liquid–solid equilibrium (i.e., the solute partition coefficient (k_0) was higher than unity) as indicated in the phase diagram [25] and therefore, in order to form of new nuclei, the liquid phase needed significant high undercooling, but the growth of the columnar grains needed minimal continued undercooling instead [25]. For the LC Ti–6Al–4V, it could be similar that epitaxial growth to form coarse columnar β phase preferably along the direction of the maximum temperature gradient (parallel to the wall build-up direction), on the previously deposited layers due to similarities in the chemical composition and surface energies of the metal [25, 44]. Subsequently, the solidified melt was transformed to the h.c.p.-structured martensitic α' phase after a rapid quenching, but retaining the prior-β columnar grain boundaries. Moreover, the martensitic α' phase also inherited the preferred orientation of the parent β columnar grains.

The formation of the grain boundaries in the LC alloys could be ascribed to the inevitable misaligned orientation between some neighboring dendritic/cellular colonies since the direction of the preferred crystallographic growth and maximum temperature gradient might not be perfectly aligned one another during the directional solidification in the LC process. Consequently, inside each colony, almost parallel columnar-like dendrites constituted small-angle boundaries; the orientation difference among the colonies was relatively large and when the growing colonies (towards their own directions of the preferred growth under the maximum temperature gradient) met each other, large-angle boundaries formed.

Rapidly solidified microstructures in metallic materials obtained by different rapid solidification processes could induce certain special material behaviors [46]. For LC materials, rapidly directionally solidified microstructures offer some unique characteristics of tensile mechanical properties such as: (1) LC materials have demonstrated almost comparable or even better yield strength ($\sigma_{0.2}$) and tensile strength (σ_{UTS}) than the corresponding ones in wrought and conventional "as-cast" condition, even though the LC materials actually should be considered as "as-cast" materials; (2) LC materials, more or less, have exhibited some anisotropic behavior in their tensile properties, particularly in their ductility. For instance, LC IN-625 alloy showed the tensile elongations (δ) of 48 and 31% along and transverse to the wall build-up direction [18]; LC IN-738 alloy showed the tensile elongations (δ) of 18 and 6.7% along and transverse to wall build-up direction [47], and LC SS316L alloys showed the tensile elongations (δ) of 43 and 35% along and transverse to wall build-up direction [18].

Effects of heat treatments in LC alloys

It is understood that the process-induced rapidly solidified microstructures in LC materials are thermodynamically metastable, which, sometimes, are beneficial to the improvement on the mechanical performance of materials. However, for high-temperature alloys such as nickel-based superalloys, the thermal stabilities of the LC microstructures and crystallographically preferred orientation at their service conditions could be a concern. Moreover, as it has been mentioned, due to the "heat sink" effect induced by

the substrate and the LC wall being built, a rapid self-quenching occurred in the LC materials immediately after solidification, that is, the "as-consolidated" LC materials could be considered as in the "as-quenched" state; therefore, for some precipitation-hardened nickel-based alloys (such as IN-718, IN-738, and Waspaloy), any precipitation of γ' (or γ'') particles from their γ matrices may be effectively suppressed or retarded. Post-heat treatments (HTs), such as the recommended standard heat treatments (SHTs) in industry [33] which have been applied for the corresponding cast or wrought nickel-based alloys, are required to ensure the LC alloys to achieve their full operational microstructures. On the other aspects, for heat-treatable LC steels (such as SS420), post-heat treatments could be used to adjust the amounts of retained austenite (γ') and carbide precipitates in order to control the dimension stability and mechanical properties such as toughness and strengths.

Nickel-based LC alloys

It is known that directionally solidified microstructures are not only likely to impart better creep rupture properties of nickel-based alloys, but their high-temperature ductility and thermal fatigue resistance would also improve further due to the reduction of the grain boundaries perpendicular to the applied stresses. The nickel-based LC alloys possess such kind of directionally solidified microstructure to provide above benefits. However, their thermal stability is a concern for practical applications. In order to assess this particular behavior of the alloys, LC IN-625 and LC IN-738 specimens have been exposed to elevated temperatures for 3–6 days to assess any evolution in their microstructures and preferred orientations.

The XRD analyses revealed that after exposure to the elevated temperatures in the range of 600–900 °C for up to 72 h, the $\gamma(200)$ diffracted line of the LC IN-625 alloy still remained as the strongest one, and the ratio of integral intensities of the diffraction lines of $I_{\gamma(200)}/I_{\gamma(111)}$ was gradually reduced from 3.7 to 1.7 (Fig. 8a) as compared to the powder one ($I_{\gamma(200)}/I_{\gamma(111)}$ was 0.5). For the LC IN-738 alloy, the preferred orientation exhibited a reasonably good thermal stability: the preferred orientation still retained after exposure to the elevated temperatures (845 °C) for more than 152 h, and the $\gamma(200)$ diffraction line was still the highest one although the ratio of $I_{\gamma(200)}/I_{\gamma(111)}$ was down from 15.8 to 4.1 (Fig. 8b).

Optical observation of the microstructures also indicated that the heat-treated LC IN-625 alloy could remain the directionally solidified dendritic structure intact up to 700 °C for 72 h (Fig. 9a); afterward, the columnar dendrites gradually disappeared; at 1100 °C the γ matrix was completely replaced by coarse columnar grains

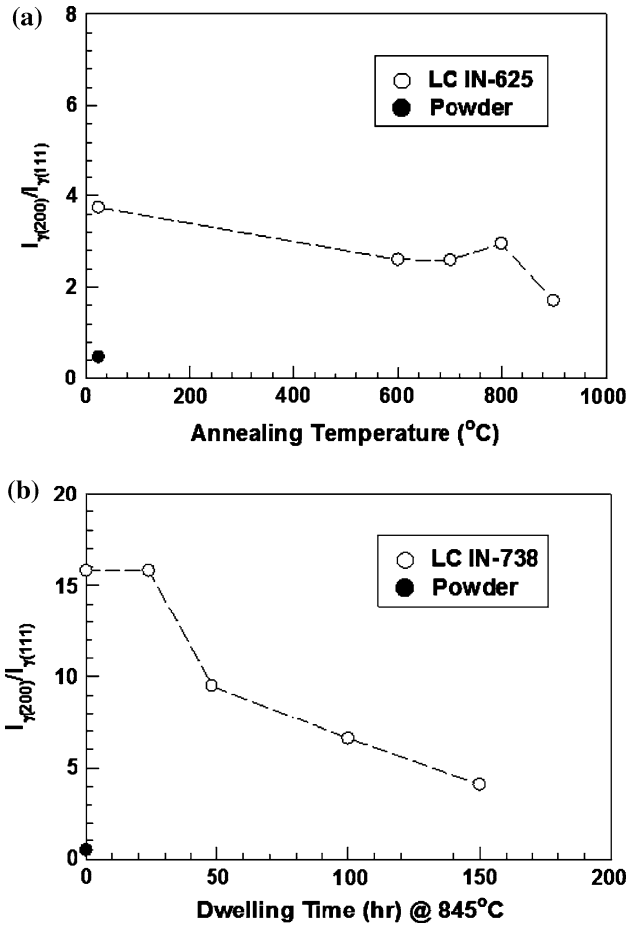

Fig. 8 The effect of heat treatment on the preferred orientation in **a** LC IN-625 (annealed at different temperatures for 72 h), and **b** LC IN-738 alloys (solutioned at 1120 °C for 2 h and aged at 845 °C for different hours), in which the $I_{\gamma(200)}/I_{\gamma(111)}$ of the powdered IN-625 and IN-738 as the baseline was 0.5

aligned with the wall build-up direction, but its preferred orientation along ⟨100⟩ still reasonably retained ($I_{\gamma(200)}/I_{\gamma(111)}$ was 1.7 against 0.5 in powder form). Figure 9b shows the SEM microstructure of the LC IN-718 alloy sectioned along the wall build-up direction after the recommended SHT. The prior directionally solidified dendrites in the LC alloy completely disappeared; while the carbides (white) presented at prior interdendritic regions and grain boundaries. Similar phenomena were observed in the LC IN-738 (Fig. 9c) and LC Waspaloy (Fig. 9d) as well. After their respective SHTs, dendrites in both LC alloys were replaced by either coarse columnar grains (LC IN-738) or equiaxial grains with twins inside (LC Waspaloy). Even so, all the nickel-based LC alloys still retained certain level of preferred orientation in their respective γ matrices even after their SHTs (see the respective $I_{\gamma(200)}/I_{\gamma(111)}$ of the XRD integral intensities in Table 4).

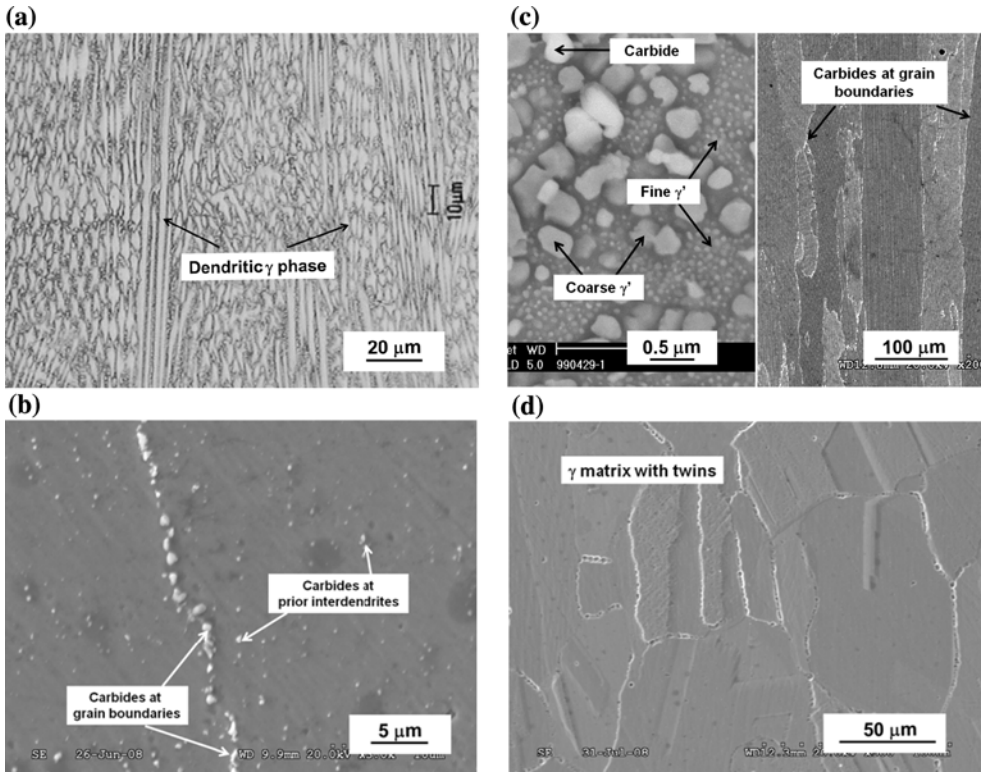

Fig. 9 Microstructures of heat-treated. **a** LC IN-625 (700 °C/72 h), **b** LC IN-718 (980 °C/1 h + 720 °C/8 h + 620 °C/8 h), **c** LC IN-738 (1120 °C/2 h + 845 °C/24 h), and **d** LC Waspaloy (1079 °C/4 h + 843 °C/4 h + 760 °C/16 h). All the specimens were sectioned along the wall build-up directions

In a short term, the process-induced preferred orientation in the nickel-based LC alloys kept relatively stable, even though it was not naturally thermodynamic equilibrium microstructure. This knowledge presents a promise in repairing/restoring damaged aerospace components since some of the parts were made by directionally solidified cast alloys to achieve better high-temperature mechanical performance, and any repaired/restored portion preserving this characteristic is desirable.

On the other hand, after the SHTs of the precipitation-hardenable nickel-based LC alloys (IN-718, IN-738, and Waspaloy), γ' (or γ'') particles should have precipitated in their respective γ matrix, which reflected on the significant increases in their yield strength ($\sigma_{0.2}$) and tensile strength (σ_{UTS}) (Table 6) since the precipitation of γ' (or γ'') particles in the γ matrix was the primary strengthening mechanism for these alloys. For the heat-treated LC IN-738 alloy, bi-modal γ' particles in the γ matrix can be observed along with fine carbides precipitated at prior interdendrites and grain boundaries with proper chemical reagent (Fig. 9c). However, the authors have failed to chemically reveal morphologies of any γ' (or γ'') particles on the matrices of the heat-treated LC IN-718 and LC Waspaloy alloys under SEM with the current chemical reagents (Fig. 9b, d).

Table 6 Effect of the recommended SHTs on tensile mechanical properties of nickel-based LC IN-718, LC IN-738 [47], and LC Waspaloy

LC material	Direction	$\sigma_{0.2}$ (MPa)	σ_{UTS} (MPa)	δ (%)
As-consolidated IN-718	L	432	802	39
SHT LC IN-718	L	1085	1238	21
As-consolidated IN-738	L	869	1202	18
SHT LC IN-738	L	869	1269	17
As-consolidated Waspaloy	L	508	797	40
SHT LC Waspaloy	L	769	1126	27

LC stainless steels

The austenitic LC SS316L, which is non-heat-treatable, has been heat treated for the purpose of investigating the stability of refined microstructure; while the martensitic LC SS420 is heat-treatable, effect of heat treatments on the tensile mechanical properties of the LC steel has been explored, and the relevance to the evolution of microstructure was studied as well.

Figure 10a shows the optical microstructures of the LC SS316L treated at 538 and 871 °C for 24 h, respectively.

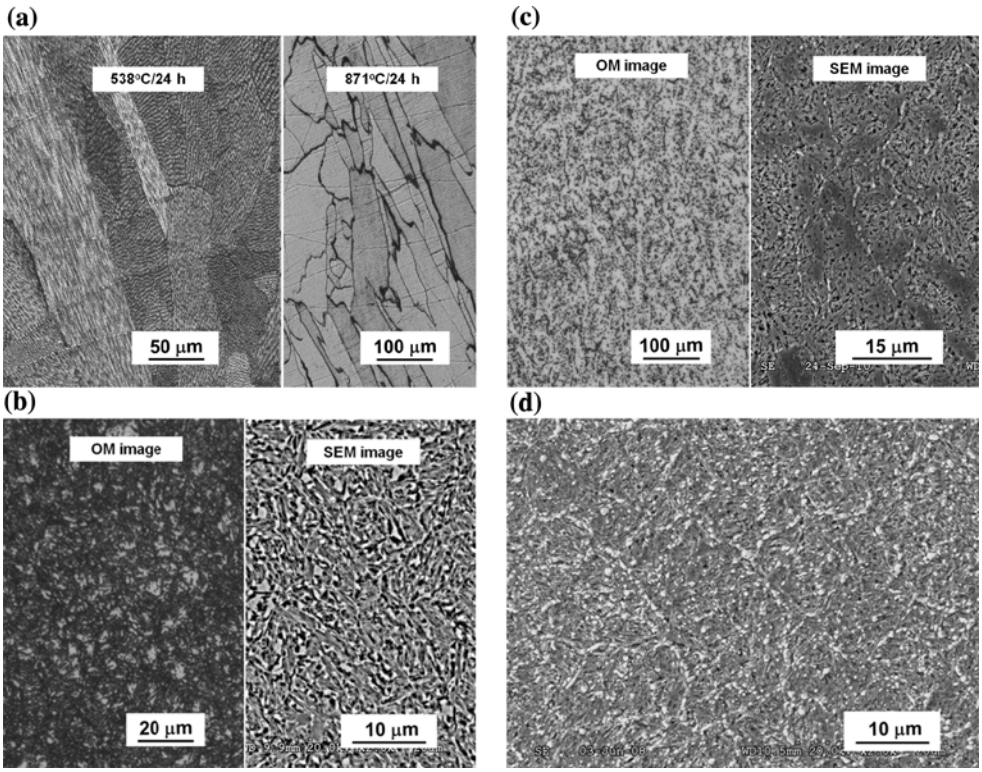

Fig. 10 Mirostructures of heat-treated. **a** LC SS316L (538 °C/24 h and 871 °C/24 h), **b** LC SS420 (316 °C/2 h), **c** LC SS420 (1008 °C/0.5 h), and **d** LC SS420 (1008 °C/0.5 h + 457 °C/2 h). All the specimens were sectioned along the wall build-up directions

Table 7 Effect of different heat treatments on tensile mechanical properties of LC SS420

LC material	Direction	$\sigma_{0.2}$ (MPa)	σ_{UTS} (MPa)	δ (%)
As consolidated SS420	L	833	1602	2.9
Wrought SS420 bar (tempered at 204 °C) [48]	n/a	1480	1720	8
SS420 (tempered at 316 °C)	L	1087	1394	1.6
SS420 (austenitized at 1008 °C and tempered at 316 °C)	L	1550	1888	2.9
SS420 (austenitized at 1008 °C and tempered at 600 °C)	L	977	1184	5.3

The former still retained fine cellular structure (with a few of columnar dendritic colonies); the latter has been replaced by non-uniform elongated coarse grains. Similar to the LC IN-625, the LC-induced refined microstructure in the LC SS316L was relatively stable (at least up to 538 °C), which subsequently could be beneficial to the improvement of relatively high-temperature mechanical properties of the material thus obtained.

Comparatively, the evolution of microstructure in the heat-treated LC SS420 inevitably affected the mechanical performance of the material. Table 7 indicates that the "as-consolidated" LC SS420 has almost comparable tensile strength (σ_{UTS}) as compared to the respective wrought one [48], but had much lower yield strength ($\sigma_{0.2}$) and elongation (δ). After directly tempered at 316 °C, the yield strength of the LC SS420 showed certain level of improvement at the expense of ultimate tensile strength and elongation. The optical and SEM microstructures of the LC SS420 tempered at 316 °C (Fig. 10b) showed that the prior dendritic structure started to dissolve, revealing characteristics of the tempered martensitic α' and retained austenitic γ' phase (reduced to about 31.8 vol.%) in the matrix. It was hard to find any presence of carbides. It should be noted that although "as-consolidated" steels (considered as "as-cast") have comparable and even better yield or tensile strength than the conventional "as-cast" or wrought one, LC steels exhibited sometimes relatively lower ductility, especially, as far as anisotropic behavior was concerned.

The mechanical characteristics of the LC steels (such as LC SS420), especially the toughness, might be related with the inherent process-induced microstructures. The post-LC heat treatments might provide an opportunity to adjust

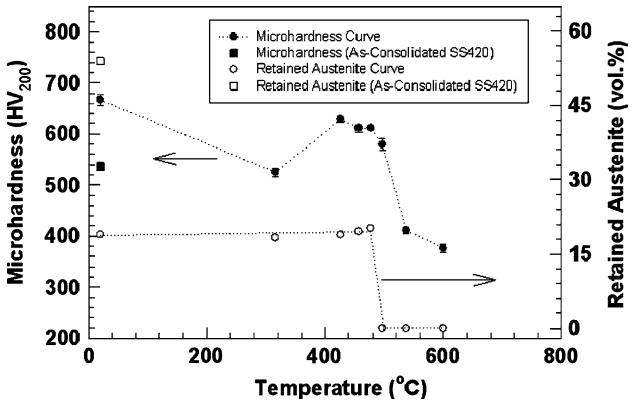

Fig. 11 The variations of volume fraction of retained austenite and microhardness of LC SS420 steel with different tempering temperatures (re-austenitizing temperature was 1008 °C)

mechanical properties of the LC materials. In the current case, the "as-consolidated" LC SS420 has been re-austenitized at 1008 °C for 0.5 h and quenched in oil in order to eliminate the presence of the dendritic structure. As the result of the re-austenization, the prior dendritic structure was indeed completely disappeared (see the optical microstructure in Fig. 10c). The "as-quenched" LC SS420 revealed a much less proportion of retained austenite (about 18.9 vol.%) as compared to the "as-consolidated" one (about 53.9 vol.%) (Fig. 11). The SEM microstructure in Fig. 10c shows that the fine carbides presented at prior interdendritic sites. Then the "as-quenched" LC SS420 has been tempered at the temperatures between 316 and 600 °C, and afterward the volumetric fraction of the retained austenite and respective microhardness of the LC SS420 were measured. Figure 11 shows that the volume fraction of retained austenite kept almost unchanged up to 477 °C, and completely disappeared at 497 °C. Meanwhile, a secondary hardening region occurred at the tempering temperature of about 427–500 °C with the maximum microhardness about 620 HV, which was primarily attributed to the precipitation and continued coarsening of fine carbides. Figure 10d shows the morphology of precipitated fine carbides in the LC SS420 re-austenitized at 1008 °C and tempered at 457 °C. Here, the tensile mechanical testing of some tempered LC SS420 has been performed as well. The results indicated that the yield strength ($\sigma_{0.2}$) and ultimate tensile strength (σ_{UTS}) of the LC SS420 austenitized at 1008 °C and tempered at 316 °C were significantly improved as compared to the respective one in "as-consolidated" condition (that is, 1150 vs. 833 MPa for $\sigma_{0.2}$, and 1888 vs. 1602 MPa for σ_{UTS}) (which were even higher than the wrought one tempered at 204 °C [48]) without compromising its elongation (δ) (remained the same as 2.9%). However, the elongation (δ) of the above heat-treated LC SS420 was still lower than the respective wrought one (2.9 vs. 8% [48]). Moreover, the elongation (δ) and yield strength ($\sigma_{0.2}$) of the LC SS420 austenitized at 1008 °C and tempered at 600 °C were improved as compared to the respective ones in "as-consolidated" condition (5.3 vs. 2.9% for δ, and 977 vs. 833 MPa for $\sigma_{0.2}$) at the expense of the tensile strength (σ_{UTS}), but the elongation (δ) was still lower than the respective wrought one (5.3 vs. 8% [48]). The improvement of elongation in the heat-treated LC SS420 could be ascribed to precipitation of fine carbides and continued coarsening at both prior inter- and intradendritic regions with increasing tempering temperature.

Conclusion

The LC process can produce metallurgically sound materials, which are free from cracks or porosities. Due to "heat sink" effect caused by the substrate and the wall being built, the process is inherent with rapid directional solidification and rapid quenching towards the LC materials, leading to some unique morphologies in their macro- and microstructures:

(1) All the "as-consolidated" LC alloys show layer-wise morphologies of solidified structures sectioned along the wall build-up direction, which reflects the "layer-up-layer" deposition.
(2) Some morphologies of solidified structures among the different LC material groups are different. All "as-consolidated" nickel-based LC alloys show coarse columnar grains in combination with dominant fine directionally solidified dendrites inside, which could span several deposited layers; "as-consolidated" austenitic LC SS316L shows spanning-multiple-layer coarse columnar grains in combination with dominant fine cellular structure inside, whereas "as-consolidated" martensitic SS420 and Al-4047 (Al–Si) aluminum alloy show that each deposited layer contains two sub-layers: one with dominated directionally solidified dendrites along the wall build-up direction and another with fine equiaxial cellular structure; and "as-consolidated" LC Ti–6Al–4V titanium alloy shows spanning-multiple-layer coarse columnar grains with no presence of any fine cellular/dendritic structure inside.
(3) The "as-consolidated" LC alloys sectioned along the wall build-up direction show more or less preferred orientation.
(4) The precipitation process in the nickel-based age-hardenable LC alloys such as LC IN-718, LC IN-738, and LC Waspaloy has been suppressed or retarded because of a rapid self-quenching immediately after

solidification. Post-heat treatments are required to achieve their operational microstructures for high-temperature performance. Moreover, for all the nickel-based LC alloys, post-heat treatments might eliminate their dendritic structures from the γ matrices, but their preferred crystallographic orientation, more or less, has been preserved.

(5) For non-heat-treatable austenitic LC SS316L, the LC-induced refined microstructure was relatively stable (at least up to 538 °C). For heat-treatable martensitic LC SS420, post-heat treatments could adjust its tensile mechanical properties. The yield or ultimate tensile strength of the LC SS420 after proper heat treatments can be equivalent to or even better than the respective wrought one. However, the elongation of the LC SS420 was always inferior to the respective wrought one under the currently investigated heat treatment schedules.

Acknowledgements The authors would like to acknowledge A. Theriault, A. Gillett, N. Santos, G. Wabersich, B. Gibson, A. Chen, and M. Meinert, NRC-IMI (London, ON), for their important contributions to the preparation of the LC specimens for metallurgical characterization and mechanical testing, and the authors are grateful to Dr. Jiaren (Jimmy) Jiang, NRC Institute for Fuel Cell Innovation (Vancouver, BC), for some useful discussion on rapid directional solidification of metals during the preparation of the manuscript as well.

References

1. Smugeresky JE, Keicher DM, Romero JA, Griffith ML, Harwell LD (1997) DOC Report #: SAND-97-8652C, USA
2. Schlienger E, Dimos D, Griffith M, Michael J, Oliver M (1998) DOC Report #: SAND-98-0664C, USA
3. Lewis GK, Nemec RB, Milewski JO, Thoma DJ, Barbe MR, Cremers DA (1994) In: ICALEO'94. LIA, Orlando, p 17
4. Mazumder J, Choi J, Nagarathnam K, Koch J, Hetzner D (1997) JOM 49(5):55
5. Mazumder J (2000) JOM 52:28
6. Abbott DH, Arcella FG (1998) Adv Mater Process 153(5):29
7. Murphy ML, Lee C, Steen WM (1993) In: ICALEO'93. LIA, Orlando, p 882
8. Toyserkani E, Khajepour A, Corbin S (2005) Laser cladding. CRC Press, Boca Raton, p 2
9. McLean MA, Shannon GJ, Steen WM (1997) SPIE 3092:753
10. Hill R, Lewis GK (1998) In: Aerospace manufacturing technology conference and exposition: Session: Emerging Processes/Affordability—Part B. SAE, Long Beach
11. Mazumder J, Dutta D, Kikuchi N, Ghosh S (2000) Opt Lasers Eng 34:397
12. Choi J, Hua Y (2004) J Laser Appl 16(4):245
13. Mazumder J (2004) US20040020625
14. Nowotny S, Scharek S, Beyer E, Richter KH (2007) J Therm Spray Technol 16(3):344
15. Huan Q, Prabhjot S, Naim AM (2008) CA2618926
16. Toyserkani E, Khajepour A, Corbin S (2005) Laser cladding. CRC Press, Boca Raton, p 8
17. Costa L, Vilar R (2009) Rapid Prototyp J 15(4):264
18. Xue L, Islam M (1998) In: ICALEO'98. LIA, Orlando, p Section E:15
19. Xue L (2006) In: Session: Additive manufacturing in aerospace manufacturing and automated fastening conference and exhibition. Toulouse
20. Xue L, Purcell CJ, Theriault A, Islam M (2001) In: ICALEO'01. LIA, Jacksonville, p 702
21. Xue L, Chen J, Wang SH, Li Y (2009) In: ICALEO'09. LIA, Orlando, (Oral presentation only)
22. Blackwell PL (2005) J Mater Process Technol 170:240
23. Pinkerton AJ, Karadge M, Syed W, Li L (2006) J Laser Appl 18(3):216
24. Wang L, Felicelli S, Pratt P (2008) Mater Sci Eng A 496:234
25. Wu X, Liang J, Mei J, Mitchell C, Goodwin PS, Voice W (2004) Mater Des 25:137
26. Kummailil J, Sammarco C, Skinner D, Brown CA, Rong K (2005) J Manuf Process 7(1):42
27. Choi J, Chang Y (2005) Int J Machine Tools Manuf 45:597
28. Chen J, Xue L (2010) Mater Sci Eng A 527:7318
29. Donachie MJ, Donachie SJ (2002) Superalloys: a technical guide, 2nd edn. ASM International, Materials Park, p 11
30. International ASM (1991) ASM handbook, heat treating, vol 4. ASM International, Materials Park, p 770
31. Donachie MJ (2000) Titanium: a technical guide. ASM International, Materials Park, p 13
32. Aluminium-Verlag Marketing and Kommunikation GmbH (1999) Aluminium handbook: fundamentals and materials, vol 1. Aluminium-Zentrale e.V, Düsseldorf, p 86
33. Donachie MJ, Donachie SJ (2002) Superalloys: a technical guide, 2nd edn. ASM International, Materials Park, p 140
34. Kahlen FJ, Kar A (2001) J Laser Appl 13(2):60
35. Pryds NH (1997) Rapid solidification of the 12%Cr steel, Risø-R-992 (EN). Risø National Laboratory, Roskile, p 39
36. Marsden CF, West DRF, Steen WM (1987) In: Proceedings of LAMP' 87. Osaka, Japan, p 401
37. Pryds NH (1997) Rapid solidification of the 12%Cr steel, Risø-R-992 (EN). Risø National Laboratory, Roskile, p 29
38. Lee JH, Kim HC, Jo CY, Kim SK, Shin JH, Liu S, Trivedi R (2005) Mater Sci Eng A 413–414:306
39. Antonsson T, Fredriksson H (2005) Metall Mater Trans B 36B:85
40. Vilar R, Conde O, Colin D (1990) In: Sudarshan TS, Bhat DG (eds) Surface modification technologies III. Miner Metals Mater Soc, Warrendale, p 343
41. Colaco R, Vilar R (1997) Scr Mater 36(2):199
42. Colaco R, Vilar R (1998) In: Sudarshan TS, Jeandin M, Khor KA (eds) Surface modification technologies XI. The Institute of Materials, London, p 600
43. Lin X, Yue TM (2005) Mater Sci Eng A 402:294
44. Semiatin SL, Kobryn PA (2001) JOM 53:40
45. Bontha S, Klingbeil NW, Kobryn PA, Fraser HL (2006) J Mater Process Technol 178:135
46. Lavernia EJ, Srivatsan TS (2010) J Mater Sci 45:287. doi: 10.1007/s10853-009-3995-5
47. Xue L, Chen J, Islam M, Pritchard J, Manente D, Rush S (2000) In: ICALEO' 00. LIA, Dearborn, p D.30
48. ASM International (1980) Metals Handbook, vol 3 (9th edn), properties and selection: stainless steels, tool materials and special-purpose metals. ASM International, Materials Park, p 27